Physicochemical Properties of Zwitterionic L- and DL-Alanine Crystals from Their Experimental and Theoretical Charge Densities

Riccardo Destro,[†] Raffaella Soave,*[,‡] and Mario Barzaghi[‡]

Dipartimento di Chimica Fisica ed Elettrochimica, Università di Milano, Via Golgi 19, 20133 Milano, Italy, and CNR-ISTM, Istituto di Scienze e Tecnologie Molecolari, Via Golgi 19, 20133 Milano, Italy

Received: October 31, 2007; In Final Form: January 17, 2008

The total experimental electron density distributions $\rho(\mathbf{r})$ of zwitterionic L- and DL-alanine crystals, as derived from extensive sets of X-ray diffracted intensities collected at 23 and 19 K, are compared to gain an insight into the different physical properties of the two related chiral compounds in the solid state and to explore the extent of the $\rho(\mathbf{r})$ transferability. Relevant parameters that characterize the two crystal forms are obtained, showing differences and similarities in terms of (i) geometric descriptors, (ii) topological indexes, (iii) molecular electrostatic potential $\Phi(\mathbf{r})$ distributions, (iv) atomic volumes and charges, (v) molecular electric moments, and (vi) electrostatic interaction energies. To assess the relative stability of the racemate with respect to the pure enantiomer, the crystal lattice energies, as obtained through DFT fully periodic calculations, are also discussed and compared with the experimental sublimation enthalpies after correction for the proton-transfer energies. In-crystal group charges, evaluated with the quantum theory of atoms in molecules, are found to be transferable between the racemic and the pure enantiomer, at variance with group volumes. Similarly, molecular first and third moments are not strictly transferable and indicate that for the zwitterionic alanine molecule the molecular charge distribution in the DL-crystal is more polarized in the *c* direction by about 10%. By contrast, quantitative agreement is observed for second and fourth moments. Significant differences arise from (1) the crystal packing of the dipole vectors, which are aligned in an antiparallel fashion in the L-crystal, to be compared with a parallel alignment in the racemate, due the polar space group $Pna2_1$ of the latter, (2) the strongly attractive electrostatic energy of a homochiral pair in the L-crystal, which is opposed to the corresponding heterochiral pair in the DL-crystal form. The difference between these E_{es} values amounts to 135−150 kJ mol^{-1}. Despite this, the two crystal forms are predicted as equally thermodynamically favored by the theoretical P-B3LYP estimates of the crystal lattice energies. Finally, the necessity of an upgrading of the dispersion and exchange-repulsion terms currently adopted within the experimental charge density approach to intermolecular interactions is recognized and discussed.

1. Introduction

A longstanding subject of chemical research is the study of the relationships between the solid-state properties and the crystal structures formed by a given compound, particularly in the case of polymorphism[1,2] and of chiral molecules that can crystallize in both an enantiomerically pure crystal structure (which contains a single D or L enantiomer) and in a racemic crystal (which contains both enantiomers). Indeed, although these crystals contain the same molecule, their structures are different: in the case of enantiomerically pure crystals, only homochiral[3] intermolecular interactions are set up between adjacent molecules, while in racemic crystals both homochiral and heterochiral interactions are formed. These diastereomeric aggregates are expected to have different energies in the crystalline state so that the racemate and the corresponding pure enantiomers may exhibit rather different physical properties.[4,5] The understanding of the key factors (geometric and/or electronic) responsible for the differences observed in related chiral compounds is a challenging task, for which a full knowledge of the nature of the intra- and intermolecular interactions in the crystals is needed, being aware that it is difficult to formulate general rules that relate crystal structures to thermochemical properties.[6,7]

In the past, the relative stability of a racemate with respect to the pure enantiomer, a topic highly relevant in the field of drug design,[8,9] has been studied by comparing their densities or their melting points[10,11] on the assumption that, the higher the value of these properties, the larger the crystal stability. Such analysis is informative, but limited:[4,12] indeed, from the literature it appears that there is not a clear trend, the racemic compound being sometimes higher melting and denser than the pure enantiomer and sometimes vice versa.[6,11] To rigorously assess the relative stability of two compounds, it is necessary to rely on quantitative thermodynamic data, when available, or on reasonable estimates of the crystal lattice energies, which are derivable from both the theoretical and the experimental charge density distributions.

In this context, a comparative study of the total charge density $\rho(\mathbf{r})$, its topological descriptors, and the related electrostatic properties (such as the electrostatic potential and the electric moments) for L and DL crystals can be highly rewarding and informative, as it allows to quantify differences and similarities among the two forms and to discover possible correlations

* To whom correspondence should be addressed. E-mail: raffaella.soave@istm.cnr.it.
[†] Università di Milano.
[‡] Istituto di Scienze e Tecnologie Molecolari.

10.1021/jp710496q CCC: $40.75
Published on Web 03/29/2008

between the physical properties and the electron density distributions.

Yet, so far the published papers dealing with the experimentally derived $\rho(\mathbf{r})$ in polymorphic structures are rather scarce,[13] and none (to our knowledge) reports a comparison between the $\rho(\mathbf{r})$ of L- and DL-crystals. Thus, the effects of unlike crystallographic environments on a given electron density are relatively understudied. This topic is intimately connected to the study of the transferability of charge distributions and derived parameters of atoms and/or fragments between chemically related compounds, currently a theme of considerable interest. Different ways have been proposed for assessing this transferability: some workers suggest the use of the multipole-model parameters as the transferable quantities,[14−16] while others[17−19] adopt the topological indicators from Bader's quantum theory of atoms in molecules (QTAIM).[20] Other approaches based on similar ideas make use of the electrostatic potential,[13c,21] the electron density shape comparison,[22] the electric moments,[23] or the Hirshfeld's surfaces and the related fingerprint plots[24] to measure molecular similarity/dissimilarity in chemically related compounds, by interpreting closer values of the property as a greater level of transferability. This point is of crucial and actual importance in the development of databases in charge density work and for the derivation of intermolecular force fields, especially when dealing with amino acids and peptides.

In this paper, we explore the structural, topological, and electrostatic features of the amino acid alanine in the crystal state, as derived from the experimental $\rho(\mathbf{r})$, with particular interest in assessing differences and similarities between the racemic (DL-alanine,[25] DLALA hereinafter) and the enantiomerically pure (L-alanine,[26,27] LALA hereinafter) crystal forms. The crystals of LALA and DLALA show the interesting feature of having very similar cell dimensions and hydrogen-bond patterns,[26] while exhibiting different densities. We note on passing that the crystal structure of DLALA represents a rare case of an amino acid racemate crystallizing in a noncentrosymmetric space group ($Pna2_1$).

In particular, we focus on these questions: (1) Which properties are more influenced by the crystal packing? (2) Which parameters are strictly transferable between LALA and DLALA? (3) Can we explain the differences in the physicochemical properties of LALA and DLALA by means of the topological analysis of the intermolecular interactions or through the study of the interaction energies? (4) Can we estimate the different energies of the homochiral (LL) and heterochiral (DL) intermolecular interactions?

The electrostatic energies of intermolecular interactions and the crystal lattice energies, as derived from the experimental $\rho(\mathbf{r})$, are also compared with theoretical results, allowing us to obtain a better understanding of the energetics in LALA and DLALA and to show benefits and drawbacks of both methods.

2. Methods

2.1. X-ray Diffraction. Full crystallographic and refinement details of our previous low-temperature crystal structure study and charge density analysis of LALA have already been reported.[27] The corresponding quantities for DLALA are given now in Table 1, together with new results for LALA, as obtained after the evaluation of the anisotropic displacement parameters (ADP's) for H atoms[28] and the refinement of a larger multipole model, including hexadecapole terms for the non H atoms and quadrupole terms for the H atoms. The same multipole model, based on Stewart formalism,[29] has been applied to DLALA.

Unit cell dimensions of the racemic crystal at 19 K (Table 1) were obtained from multiple measures of several setting angles on a modified[30] four-circle Syntex $P\bar{1}$ diffractometer equipped with a Samson cryostat.[31] All X-ray diffraction intensities were measured on this instrument, and their multipole refinements were carried out with the VALRAY[32] code.

TABLE 1: Crystallographic and Refinement Details

	LALA	DLALA
Sample Information		
empirical formula	$C_{12}H_{12}O_5$	
crystal size/mm^3	0.18 (radius of a sphere)	0.45 × 0.25 × 0.14
formula wt/g mol^{-1}	89.097	
crystal system	Orthorhombic	
space group	$P2_12_12_1$ (No. 19)	$Pna2_1$(No. 33)
Z	4	
T/K	23 (1)	19 (1)
a/Å	5.9279(10)	11.9140(13)
b/Å	12.2597(17)	5.9590(9)
c/Å	5.7939(9)	5.8388(6)
V/Å^3	421.1(1)	414.53(9)
D_X/g cm^{-3}	1.405	1.428
$F(000)$	192	
μ/mm^{-1}	0.11	
Data Collection		
λ/Å	0.71073	
$(\sin\vartheta/\lambda)_{max}$/Å^{-1}	1.08	1.15
no. collected reflns	5885	12624
no. unique reflns	2535	2785
no. obsd reflns ($I > 0$, N_{obs})	2519	2748
Refinement Results		
GoF	1.0633	1.0711
$R(F)$, $R(F^2)^a$	0.0195, 0.0211	0.0183, 0.0192
$R_w(F^2)^a$	0.0289	0.0268
$R(F)$, $R(F^2)^b$	0.0088, 0.0138	0.0084, 0.0139
$R_w(F^2)^b$	0.0171	0.0181
no. variables (N_v)	268	267
N_{obs}/N_v	9.4	10.3

[a] R values for all data. [b] R values for data with $\sin\theta/\lambda \leq 0.65$ Å^{-1} (591 for LALA, 521 for DLALA).

The relevance of including atomic ADP's for the H nuclei in the least-squares multipole model has been recently stressed[33] as crucial in electron density studies of molecular crystals, because a proper description of the H atoms is critical for both the molecular electrostatic properties and the chemical reactivity.

2.2. Theoretical Calculations. Single-point calculations have been performed on the alanine molecule extracted from both the LALA and DLALA crystals and on three hydrogen-bonded isolated molecular pairs of both the crystal forms at the low-temperature (LT) experimental geometry. The ADF2004.01[34,35] program has been used, adopting the standard triple-ζ exponential (TZP) basis set and the BLYP[36,37] functional, within the generalized gradient approximation (GGA). The dimer interaction energies have been calculated taking into account the correction for the basis set superposition error (BSSE) by the counterpoise method.[38] The LT experimental geometries of LALA and DLALA have been used as starting points for the DFT optimizations of the isolated molecules with the Gaussian98 (G98) program, adopting the B3LYP[37,40] hybrid-type functional and the double-ζ plus polarization (DZP) basis set.[41,42] The relaxation energy E_{rel} has been calculated as the difference between the energy of the optimized isolated molecule (neutral form) and the energy of the molecule at the crystal geometry (zwitterionic form) and therefore includes the energetic contribution due to the intramolecular proton transfer.[43,44]

Fully periodic DFT calculations at the LT experimental geometry were then carried out with the CRYSTAL03 program.[45] The same exchange and correlation functionals and the same basis set as in the G98 calculations have been adopted,

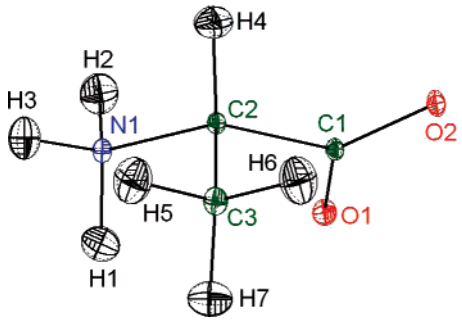

Figure 1. ORTEP plot of the alanine molecule in the DLALA crystal at 19 K with the atom numbering scheme. Ellipsoids are at 50% probability level.

according to recent suggestions for periodic calculations on molecular crystals.[46] In the following and in the tables the notations MG-B3LYP and MA-BLYP are used to distinguish molecular calculations (with G98 and ADF, respectively) from those on the periodic crystal, which are marked as P-B3LYP.

The lattice energy E_{latt} is defined as

$$E_{latt} = E_{crystal}/Z - E_{molecule} \quad (1)$$

where $E_{crystal}$ is the crystal energy per unit cell, Z is the number of molecules per unit cell, and $E_{molecule}$ is the energy of the isolated molecules at the crystal geometry. Both these energies have been evaluated with the CRYSTAL03 program.[45] The BSSE in E_{latt} has been corrected by the counterpoise method,[38] adding the basis sets of all ghost atoms at a distance less than 3.5 Å from the molecule in the $E_{molecule}$ calculations. Both ZPE contributions to the lattice energy and crystal geometry optimizations were ignored.

The analysis of the experimental and theoretical $\rho(\mathbf{r})$ in terms of (i) topological features, (ii) nuclear-centered distributed multipole analyses (DMA), and (iii) derived electrostatic properties was performed by means of the program PAMoC (an acronym for properties of atoms and molecules in molecular crystals),[47] which retrieves all the required information from either the binary checkpoint file produced by VALRAY or the AIMPAC wavefunction files[48] generated by G98 and ADF.

3. Results and Discussion

3.1. Molecular Conformation and Crystal Packing. An ORTEP plot of the alanine molecule in the crystal of DLALA at 19 K is shown in Figure 1,[49] while full lists of experimental bond distances, bond angles, and torsion angles of both LALA and DLALA at 23 and 19 K, respectively, are reported in the Supporting Information. In both the crystal structures, the standard uncertainties (s.u.) are ≤0.0005 Å for bond distances, ≤ 0.03° for bond angles, and ≤0.07° for torsion angles, when only non-H atoms are implied. In spite of the low s.u. for the bond lengths, corresponding bonds in LALA and DLALA never differ by more than 3.7 s.u. The significant disparity already observed[25a,26,27d] between the two C−O bond distances of LALA is confirmed by our data on DLALA, where the C1−O2 bond is 0.02 Å longer than the C1−O1 bond. The C−COO$^-$ fragment is planar in both the crystals, the central carbon atom C1 lying 0.0024 Å (LALA) or 0.0028 Å (DLALA) on one side and O1, O2, and C2 less than 0.001 Å on the other side of the mean plane. Bond angles are likewise very similar in LALA and DLALA, with the exception of the two C−C−O angles: their asymmetry, already noted in the case of LALA[27d] (118.32° for C2−C1−O1 vs 115.88° for C2−C1−O2), is even more marked in DLALA (118.77 vs 115.33°, respectively), indicating a slightly different relative orientation of the carboxyl group with respect to the C1−C2 bond in the two structures. But the most striking difference is shown for the two sets of four torsion angles that describe the molecular conformation of alanine in the crystals of LALA and DLALA, respectively; each of the four dihedral angles differs, in the two crystal structures, by 2.6−2.8° (on average, about 80 s.u.), revealing that the different molecular environment in the two crystals substantially affects the molecular conformation of the alanine molecule, although leaving almost unchanged the bond geometry.

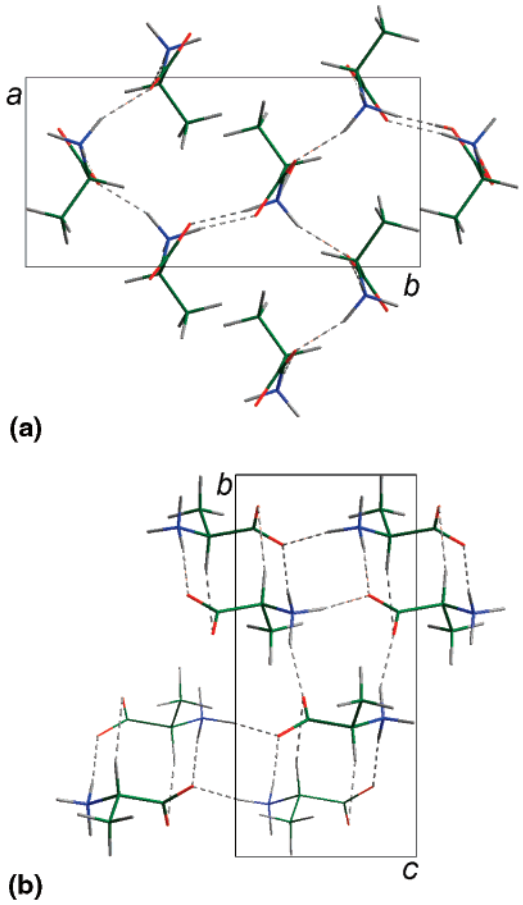

Figure 2. Packing diagram of LALA, viewed down (a) the *c* axis and (b) the *a* axis. Intermolecular interactions are represented as dashed bonds.

As noted by Simpson and Marsh[26] in the first comparison of the crystal packings of LALA and DLALA, the two crystal structures have very similar cell dimensions and supramolecular organization, despite the different space groups (Table 1). Indeed, the projected structures along the *c* axis are virtually identical, provided that the *a* and *b* axes are interchanged, and the packing motifs are in both cases characterized by a network of head-to-tail hydrogen-bond sequences (Figures 2 and 3).

The geometrical parameters of the two sets of NH···O hydrogen bonds (Table 2) show strong short-range structural similarity, including extremely similar H-bonds lengths, with differences between the same bonds never exceeding 1.6 s.u. The main discrepancy between the two structures is that, while in LALA the three hydrogen-bonded dimers (pairs A, B, and C, see Figure 4) are homochiral and all arranged in a head-to-tail fashion, in DLALA the glide plane *n* perpendicular to the *a*-axis gives rise to the heterochiral pair B with a head-to-head arrangement. The latter is expected to be less stabilized by electrostatics than the same pair in LALA, in spite of the

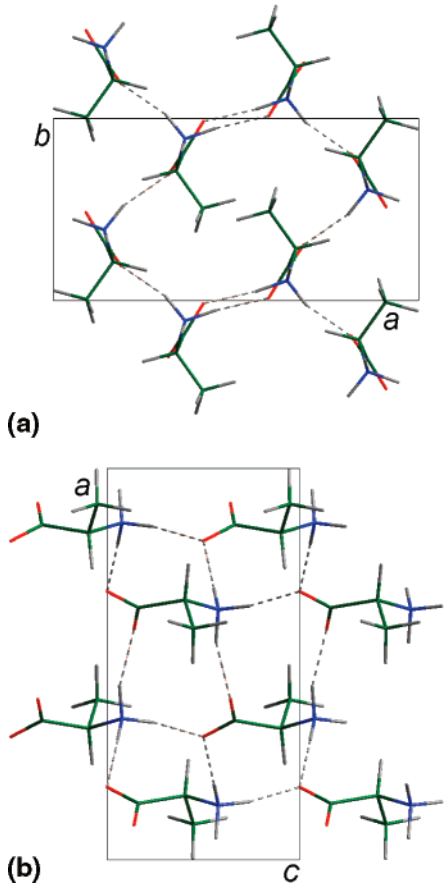

Figure 3. Packing diagram of DLALA, viewed down (a) the *c* axis and (b) the *b* axis. Intermolecular interactions are represented as dashed bonds.

geometrical similarity between the formed N1−H2···O2 hydrogen bonds.

3.2. Intra- and Intermolecular Topological Properties. Bader's QTAIM[20] is a well-established tool to fully characterize chemical interactions and to obtain a quantitative determination of their strength, especially in the case of hydrogen-bonded crystals.[50] Full lists of the topological properties at the bond critical points (bcps) of LALA and DLALA are reported in the Supporting Information. Figure 5 shows the experimental values of $\rho(\mathbf{r})$ and $\nabla^2\rho(\mathbf{r})$ at the bcps for the covalent bonds of LALA and DLALA: the lower bars show $\rho(\mathbf{r})$ values at the bcps (dark gray for LALA and light gray for DLALA), while the upper bars display $\nabla^2\rho(\mathbf{r})$ values at the same bcps (dark blue for LALA and light blue for DLALA). An overall good consistency is found, fully confirming the results recently reviewed by Koritsanszky and Coppens[51] regarding a series of experimental ρ_{bcp} and $\nabla^2\rho_{bcp}$ values of bonds common to 11 amino-acids: these local topological indices spread over a narrow range in amino acids and are therefore generally transferable. Our data on LALA and DLALA never differ by more than 4 s.u., with the exception of the ρ_{bcp} values at the C1−C2 bond ($\Delta = 5$ s.u.) and of the $\nabla^2\rho_{bcp}$ values at the C1−O1 bond ($\Delta = 4.5$ s.u.). The value of the Laplacian at the bcp for this bond in DLALA is more negative by 14 eÅ^{-5} than the average value reported in the above-mentioned review,[51] corresponding to almost 3 root-mean-square deviations, further suggesting that the Laplacian for the C−O bonds of the carboxylate group is not completely reproducible.

As to the values of the bond ellipticity ϵ, defined as $(\lambda_1/\lambda_2) - 1$ and usually reported as the least reproducible descriptor, we found global excellent agreement between LALA and DLALA values, which never differ by more than 3 s.u., the only exception being ϵ for the C2−C3 bond ($\Delta = 5$ s.u.). This picture allows us to conclude that, from the point of view of the local, intramolecular topological properties, the molecules of LALA and DLALA do not significantly differ, despite the diverse molecular conformation and crystallographic environment.

From inspection of Table 2, which lists the contact geometry and the topological parameters of the most relevant XH···O (X = N, C) intermolecular interactions in pairs A, B, and C of LALA and DLALA, some information can be obtained on the influence of the different packings on the strength of the H bonds in the two zwitterions. Together with the experimental values of $\rho(\mathbf{r})$ and $\nabla^2\rho(\mathbf{r})$, at each bcp we report also the estimated potential energy density $V(\mathbf{r})$,[52,53] a quantity that we consider as a valuable descriptor of the strength of the H-bonds.[54] We note that: (1) In pair A the three topological parameters for the N1−H3···O2 hydrogen bond are equal, within 2.5 s.u., in LALA and DLALA; they describe both interactions as strong and virtually identical also on a topological ground. (2) The same holds for pair C, although the N1−H1···O1 H bonds of this pair are weaker than the N1−H3···O2 H bonds of pair A. (3) Pair B shows a slightly different feature: the values of the topological parameters at the bcps of the N1−H2···O2 interactions in LALA and DLALA differ up to 5 s.u. and depict the H bond in DLALA stronger than that in LALA and comparable with the N1−H3···O2 H bonds of pairs A. However, in LALA the head-to-tail orientation of the molecules in pair B is such as to allow the formation of an additional C2−H4···O1 bonded interaction, which is expected to contribute to the stabilization of the pair.

All this indicates that the gross features of the hydrogen-bonding pattern in LALA and DLALA are substantially comparable from both a geometrical and a topological point of view.

3.3. Electrostatic Potential. It is well-known that one of the most useful applications of experimental charge densities, especially in the field of biologically significant compounds, is the derivation of the molecular electrostatic potential $\Phi(\mathbf{r})$,[51] for its ability to predict the molecular reactivity and the strength of intermolecular interactions[51,55] and to reveal the effects of different crystallographic environments on the electron densities of individual molecules.[13c,21] Figure 6 shows the experimentally derived $\Phi(\mathbf{r})$ for both LALA and DLALA mapped with the program MolIso[56] onto the isodensity surfaces of 0.00675 e Å^{-3} (this particular value is one of the most commonly occurring in the literature[21] and the one that Bader proposed in his original work on molecular surfaces[57]).

Both the maps exhibit a great charge separation, as expected, with a large pronounced electronegative area around the COO^- moiety separated from a similarly sized electropositive surface, a clear evidence of the overall dipolar nature of the zwitterions in the crystal state. While the overall features of $\Phi(\mathbf{r})$ in LALA and DLALA are comparable, some differences can be observed in terms of the molecular surface shape and of the position of the maxima of $\Phi(\mathbf{r})$: (1) In DLALA the electropositive region is larger than in LALA, and the surface shape around the H1 atom is more pronounced, showing that the different environment in the crystal has effectively changed the electron density distribution of the molecules. (2) The strongest positive regions of $\Phi(\mathbf{r})$ (deep violet in Figure 6) are not equally distributed around the acidic H atoms. As a consequence, the likely directions of approach of nucleophilic reactants toward LALA and DLALA are predicted as slightly different. Conversely, the

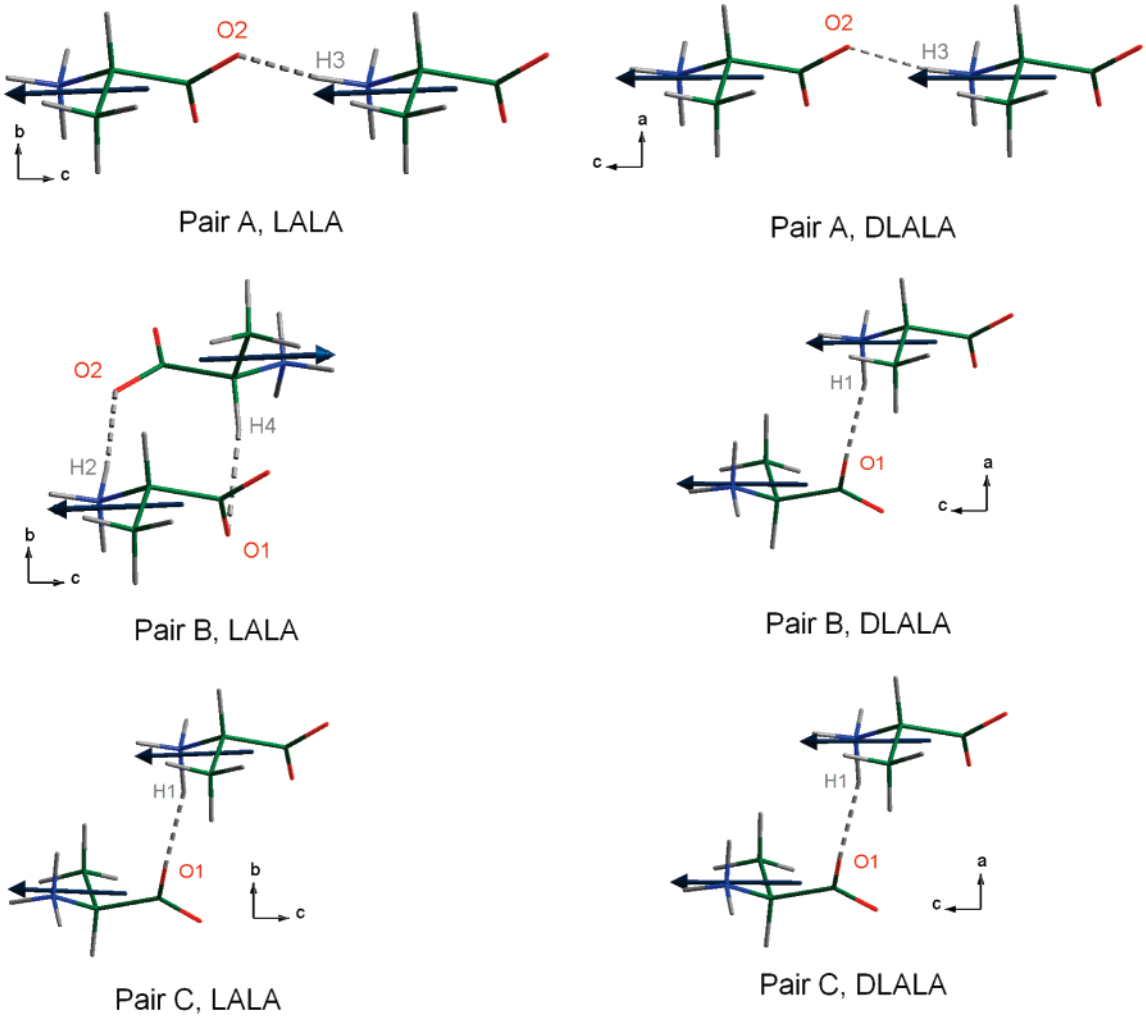

Figure 4. Molecular plot of the three hydrogen-bonded dimers of LALA and DLALA, the μ_{exp} direction being indicated.

TABLE 2: Experimental Contact Geometry and Topological Parameters of the Most Relevant XH···O (X = N, C) Interactions in Crystals of LALA and DLALA

pair	crystal	contact	HO/Å	XH/Å	XO/Å	XHO/°	$\rho(\mathbf{r})_{bcp}$ [a]	$\nabla^2[\rho(\mathbf{r})_{bcp}]$[a]	$V(\mathbf{r})$[b]
A	LALA	N1−H3···O2[c]	1.765(10)	1.039(11)	2.7921(4)	169.2(7)	0.29(2)	2.8(4)	−104(5)
	DLALA	N1−H3···O2[d]	1.781(10)	1.017(10)	2.7890(4)	170.6(8)	0.28(2)	1.9(4)	−91(5)
B	LALA	N1−H2···O2[e]	1.814(9)	1.036(9)	2.8140(4)	161.0(8)	0.25(1)	1.7(2)	−79(4)
	LALA	C2−H4···O1[f]	2.393(8)	1.085(8)	3.4382(4)	161.2(5)	0.07(1)	0.94(6)	−15.8(9)
	DLALA	N1−H2···O2[g]	1.802(7)	1.019(7)	2.7933(3)	163.1(6)	0.30(1)	2.1(3)	−104(5)
C	LALA	N1−H1···O1[h]	1.842(10)	1.029(10)	2.8341(4)	160.8(7)	0.22(1)	2.1(2)	−70(3)
	DLALA	N1−H1···O1[i]	1.840(8)	1.045(7)	2.8503(3)	161.5(7)	0.24(1)	1.9(2)	−77(4)

[a] The units are e Å^{-3} for the charge density and e Å^{-5} for the Laplacian. S.u. in parentheses. [b] In units of kJ mol^{-1} per atomic unit volume. [c] At $x, y, -1 + z$. [d] At $x, y, 1 + z$. [e] At $^1/_2 + x, ^1/_2 - y, 1 - z$. [f] At $-^1/_2 + x, ^1/_2 - y, 1 - z$. [g] At $^1/_2 - x, ^1/_2 + y, ^1/_2 + z$. [h] At $^3/_2 - x, -y, -^1/_2 + z$. [i] At $-x, 1 - y, ^1/_2 + z$.

minima of $\Phi(\mathbf{r})$, amounting to −478(40) and −514(53) kJ mol^{-1} for LALA and DLALA, respectively, are the same within 1 s.u, and the O2 atom is the closest atom to the minimum in both the cases (1.118 and 1.221 Å apart, respectively).

3.4. Atomic Volumes. Bader's QTAIM[20] provides a unique *discrete* boundary partitioning of the real space of a molecule or a crystal into submolecular regions, fragments or single atoms, whose atomic or group properties (like volumes and charges) are additive and well suited to investigate transferability. The calculation of these properties from an experimental or a theoretical charge distribution of amino acids is of great importance in protein engineering studies, as amino acids are the constituting building blocks of proteins. In our study, the *in-crystal* QTAIM atomic volumes, V_{cry}, of the zwitterionic LALA and DLALA are defined by the interatomic boundaries in the crystal, while atomic volumes of a single molecule extracted from the crystal, denoted by V_{001}, are based on a cutoff of $\rho = 0.001$ atomic units. The results are reported as group volumes in Table 3. It appears that this is the first time that QTAIM volumes and charges for zwitterionic amino acids are reported, as previous results in the literature all refer to the non-zwitterionic form $HOOCC_\alpha HRNH_2$.[18,19,58−60] From inspection of Table 3 it can be seen that: (1) In both LALA and DLALA the NH_3^+ group is subject to a significant volume reduction (by ca. 14 and 20%, respectively) when passing from the molecule to the crystal, due to the involvement of the acidic H1, H2, and H3 atoms in the formation of the intermolecular H bonds. (2) The V_{001} volumes of the terminal methyl groups of LALA and DLALA (second row in Table 3) are virtually equal and suggest transferability of this property between the

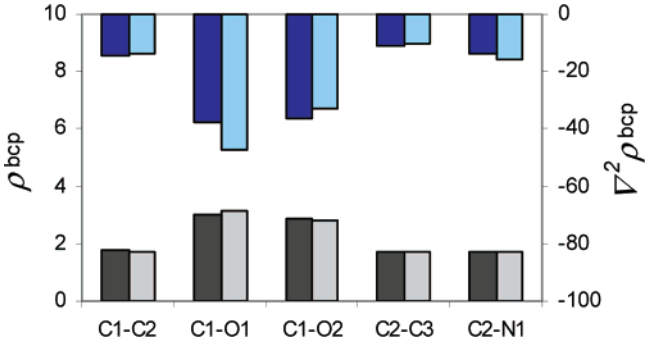

Figure 5. Electron density and Laplacian at the bcps for LALA and DLALA. The lower bars show $\rho(\mathbf{r})$ values at the bcps (dark gray for LALA and light gray for DLALA), while the upper bars display $\nabla^2\rho(\mathbf{r})$ values at the same bcps (dark blue for LALA and light blue for DLALA).

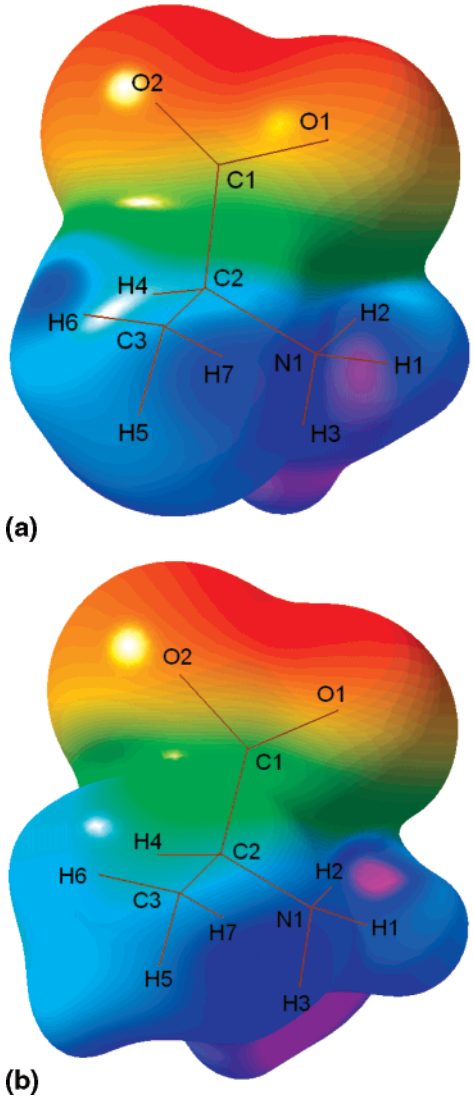

Figure 6. Molecular electrostatic potential mapped on the isodensity surface of 0.00675 Å^{-3} for the alanine molecule in crystals of (a) LALA and (b) DLALA. The color scheme ranges from red (negative) via green (neutral) to blue (positive) with values in the range −410 → +456 kJ mol^{-1}.

isolated molecules, but the corresponding V_{cry} values differ by more than 4%, indicating that the basin of the methyl group is not the same in the crystals of LALA and DLALA (hence not strictly transferable). (3) This holds also for the V_{cry} volumes of the NH_3^+ groups, whose difference between LALA and DLALA amounts to more than 5%. (4) Conversely, the COO^- and CH atom groupings are almost identical in LALA and DLALA, showing that they are less influenced by the crystal packing. (5) For LALA the sum of the V_{001} atomic volumes amounts to 105.67 Å,^{3} while the molecular volume in the crystal, given by $\Sigma_\alpha V_{cry,\alpha}$, amounts to 103.95 Å^3 with a reduction of 1.6%. The same values in DLALA amount to 105.75 and 101.65 Å,^{3} respectively, with a reduction of 3.9%. This is further evidence that the molecules of LALA and DLALA, when extracted from the crystals, are substantially identical, while, when properly packed in their crystal system, they are affected by different crystallographic environments and occupy different volumes.

TABLE 3: Experimental Group Volumes (Å^3) from QTAIM Partitioning of the Electron Density (First Row, In-Crystal Values, with Molecular Boundaries Defined by the Interatomic Zero-Flux Surfaces in the Crystal; Second Row, Values for Molecules Extracted from the Crystal, Based on a Cutoff of $\rho = 0.001$ Atomic Units)[a]

group	LALA	DLALA
COO^-	40.13	40.25
	39.78	39.98
NH_3^+	20.50	19.40
	23.79	24.22
CH	13.26	13.24
	13.39	13.15
CH_3	30.06	28.76
	28.71	28.41
molecule	103.95	101.65
	105.67	105.75

[a] The reliability and accuracy of the integration procedure amount to 1.2 and 1.9% for LALA and DLALA, respectively.

All these findings indicate that the extent of the transferability of in-crystal atomic volumes is not as convincing as in other studies[19,59] and suggest that the alanine molecule is more modified when packed in the racemic crystal form than in the pure enantiomorph. Full lists of the QTAIM atomic volumes are reported as Supporting Information.

3.5. Atomic Charges. Within Bader's QTAIM, unabridged Cartesian moments of the charge density, $\boldsymbol{m}_\alpha^{(l)}$, are obtained by integrating the moment operator $x^i y^j z^k$ of rank $l = i + j + k$ ($i, j, k = 0, 1, 2, 3$) inside the atomic basin, Ω_α, of atom α[61]

$$\boldsymbol{m}_\alpha^{(l=i+j+k)} = \int_{\Omega\alpha} x^i y^j z^k \rho(\mathbf{r})\, d\mathbf{r} \qquad (2)$$

The zeroth-rank moment $m^{(0)}_\alpha = p^{(0)}_\alpha$ gives the atomic population, i.e., the total number of electrons, of atom α. Hereinafter it will be replaced by the atomic net charge $q_\alpha = Z_\alpha - m^{(0)}_\alpha$, where Z_α defines the nuclear charge of atom α.

The experimental $\rho(\mathbf{r})$ of LALA and DLALA have been analyzed in terms of the QTAIM distributed multipole analysis (DMA), and the results are reported as group charges in Table 4 and as full lists in the Supporting Information. The value of the integral $L(\Omega) = \int_\Omega \nabla^2\rho(\mathbf{r})d\tau$ was checked and shown to be less than $\pm 0.5 \times 10^{-3}$ a.u. At variance with group volumes, corresponding group charges in LALA and DLALA never differ by more than 2 s.u.: this holds for both q_{cry} and q_{001} values (first and second row in Table 4, respectively), pointing to a larger transferability of this property with respect to atomic volumes. It can be seen that the COO^- and NH_3^+ groups become more charged in modulus (by about 10 and 20%, respectively) when the interatomic boundaries in the crystal are taken into account ($q_{cry} > q_{001}$). This feature is more marked in DLALA than in LALA, and this result reflects the increased polarization

TABLE 4: Experimental Group Charges (Electrons) from QTAIM Partitioning of the Electron Density (First and Second Row as in Table 3)

group	LALA	DLALA
COO^-	−0.92(3)	−0.94(4)
	−0.85(3)	−0.85(3)
NH_3^+	0.38(3)	0.36(3)
	0.33(3)	0.29(3)
CH	0.37(2)	0.36(3)
	0.37(2)	0.35(3)
CH_3	0.17(3)	0.22(4)
	0.15(3)	0.21(4)

TABLE 5: Experimental Molecular Dipole Moment (μ, Debye) from QTAIM Partitioning of the Electron Density (First and Second Row as in Table 3)[a]

	LALA	DLALA
$\|\mu\|$	13.3(3)	14.7(6)
	12.4(3)	13.7(6)
μ_x	−13.1(3)	−14.5(6)
	−12.3(3)	−13.5(6)
μ_y	1.9(3)	1.8(3)
	1.8(3)	1.4(3)
μ_z	1.0(1)	1.6(2)
	0.9(2)	1.4(2)

[a] The component values refer to the inertial coordinate system with origin in the center of mass. Experimental s.u. are in parentheses.

of the COO^- and NH_3^+ groups due to the formation of the intermolecular hydrogen bonds.

3.6. Molecular Electrostatic Moments. Electric moments provide a compact summary of the molecular charge distribution, giving some insight into the nuclear and electronic structures of molecules and into the rationalization of intermolecular interactions.[62] They can be derived with great accuracy from both theoretical calculations and X-ray diffraction experiments of charge density quality[51,62] and can be used to measure molecular similarity/dissimilarity in chemically related compounds by interpreting closer values of the property as a greater level of transferability. This has been done, for example, for the whole series of amino acid side chains through ab initio calculations on the neutral amino acid model HC(═O)|NHC_αH-(R)C−(═O)|NH_2.[23]

Molecular electrostatic moments of LALA and DLALA have been calculated up to the fourth rank, by shifting all atomic moments $\boldsymbol{m}_\alpha$ to a common origin,[63] the center of mass of the molecule, and then summing the results together

$$\boldsymbol{m}_{\mathrm{mol}} = \Sigma_\alpha \boldsymbol{S}_\alpha(\boldsymbol{R}_\alpha - \boldsymbol{R}_o)\boldsymbol{m}_\alpha \qquad (3)$$

The shift matrices $\boldsymbol{S}_\alpha(\boldsymbol{R}_\alpha - \boldsymbol{R}_o)$ depend on the Cartesian coordinates of the nuclear center α, $\boldsymbol{R}_\alpha$, and of the molecular center of mass, $\boldsymbol{R}_0$. It has to be noted that two different results for the molecular moments $\boldsymbol{m}_{\mathrm{mol}}$ are obtained, if a QTAIM discrete partitioning of periodic electron densities is adopted, depending on the definition of molecular boundaries. When molecular boundaries are moved artificially to infinity, the molecule is extracted from the crystal and QTAIM molecular moments are identical to Stewart molecular moments[29] within numerical accuracy. On the other hand, when molecular boundaries are defined by the interatomic boundaries in the crystal, then the real *in-crystal* molecular moments are obtained.

3.6.1. Dipole Moments. Molecular first moments of LALA and DLALA, based on QTAIM partitioning of their experimental electron densities, are listed in Table 5, with all components expressed in the inertial reference system of coordinates and the origin placed at the centers of mass of the molecules. From the QTAIM partitioning of the experimental $\rho(\mathbf{r})$ applied to the molecules extracted from the crystals, values of 12.4(3) and 13.7(6) D have been found for the magnitude of the dipole moment of LALA and DLALA, respectively. These values, basically dominated by large net charges on COO^- and NH_3^+ groups, increase up to 13.3(3) and 14.7(6) D, respectively, when the QTAIM partitioning is applied to the molecules in the crystals, the increment of 7% representing the polarization of the electron density in the crystal. The molecular charge distribution of DLALA appears to be more polar than the $\rho(\mathbf{r})$ of LALA by about 1.3 D (10%), even if in terms of standard uncertainty (s.u.) this difference is scarcely significant. As expected, the direction of the in-crystal dipole moment is approximately parallel to the principal axis of the molecule (as observed also in the case of glycine[64]), and to the *c* axes of the crystals, the angle between the latter and the dipole vector amounting to 2.1 and 3.4° for LALA and DLALA, respectively. All these findings indicate that the amino acid molecule roughly maintains the same dipolar nature in LALA and DLALA, and the small changes here discussed measure the extent of their transferability.

However, due to the diverse space groups of LALA and DLALA ($P2_12_12_1$ and $Pna2_1$, respectively), the way in which their molecular dipole moments pack in the crystals is significantly different (Figure 7). The crystallographic (*b*,*c*) plane in LALA and the (*a*,*c*) plane in DLALA, because of the interchange between the *a* and *b* axes, are "equivalent": in these projections head-to-tail chains of dipoles are formed along the *c*-axis in both the structures, with molecules related by translations along *c*. Conversely, in the other direction (i.e., along *b* in LALA and along *a* in DLALA), the packing patterns are different: in LALA the molecules are related by 2-fold screw axes and adjacent rows of dipoles arrange themselves in an antiparallel fashion (maximizing their electrostatic attractive energy), while in DLALA the molecules are related by n-glide operations and adjacent rows of dipoles are parallel aligned. The latter architecture is common to all the crystal structures that crystallize in polar space groups such as the $Pna2_1$, having the molecular dipoles parallel or nearly parallel to the polar axis. As a consequence, the unit cell has a nonzero dipole moment and an additional term for the Coulombic energy must be considered when estimating the lattice energy[65] (see section 3.8).

3.6.2. Higher-Order Moments. They are graphically visualized in Figure 8 through linear correlations between the experimental in-crystal QTAIM values of the individual components for LALA and DLALA, with the aim of quantifying the molecular similarity/dissimilarity in terms of these properties. It can be seen that: (1) For the second moments the slope is equal to 1.00(3), indicating a quantitative agreement between the values of the tensor components of LALA and DLALA and suggesting a marked similarity of this property in the two crystals (Figure 8a). (2) In Figure 8b the components $v_i = \Sigma_j m_{ijj}$ ($i,j = x,y,z$) and the magnitude $|v|$ of the vector part of the third moment tensors are also reported: the latter have roughly the same orientation of the molecular dipole vectors (the angles between the two vectors amounting to 16° and 12° for LALA and DLALA, respectively) and are, as expected, large and highly significant, further reflecting the dipolar nature of the charge distribution of the zwitterionic alanine. The v_x value of DLALA is larger than the corresponding value in LALA by about 20%, corroborating the trend observed for the group charges and the first moments and confirming that the charge distribution in crystals of DLALA is more polarized in the *c* direction than in

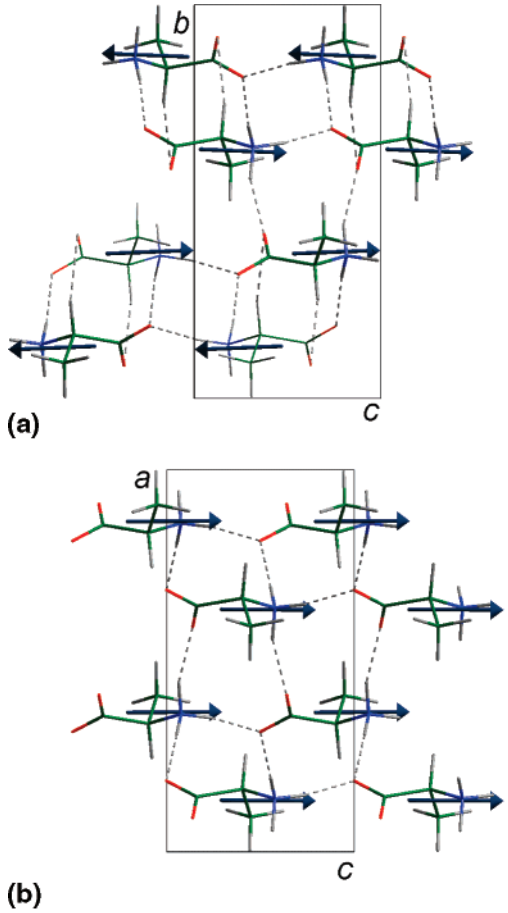

Figure 7. (a) LALA, crystal packing view along *a*, the experimental molecular dipole moment direction being indicated. Dashed lines represent the hydrogen bonding in the *bc* plane. (b) DLALA, crystal packing view along *b*, the experimental molecular dipole moment direction being indicated. Dashed lines represent the hydrogen bonding in the *ac* plane.

LALA. This is also reproduced by the value of the slope of the least-squares straight line of Figure 8b, which is significantly larger than 1. (3) On the other hand, the slope of the linear correlation of the fourth moment components (Figure 8c) is slightly smaller than 1: in this case the difference from unity is scarcely significant, pointing to a substantial similarity between the fourth moments of LALA and DLALA.

3.7. Electrostatic Energies of Intermolecular Interactions. For crystals containing polar molecules, the electrostatic interaction energies E_{es} between molecules are one of the most significant contributions to the total binding energies[43,51,64] and hence play a key role in the stabilization of the formed crystal structures. Theoretical and experimental estimates of E_{es} for the three hydrogen-bonded molecular pairs of LALA and DLALA (Figure 4) are summarized in Table 6. The fourth column reports the experimental values of E_{es} as obtained from the multipolar X-ray $\rho(\mathbf{r})$ through the Buckingham-type (moment−moment, MM) approach,[66] corrected for the promolecule energy, following the strategy recently proposed by Spackman[67] and implemented in the code PAMoC.[47] In this approach, the E_{es} is expressed as a sum of promolecule−promolecule, promolecule−deformation, and deformation−deformation terms

$$E_{es} = E_{pro-pro} + E_{def-def} + E_{pro-def} \quad (4)$$

The $E_{pro-pro}$ term involves a sum over Coulombic interactions between pairs of spherical atomic charge densities and can be

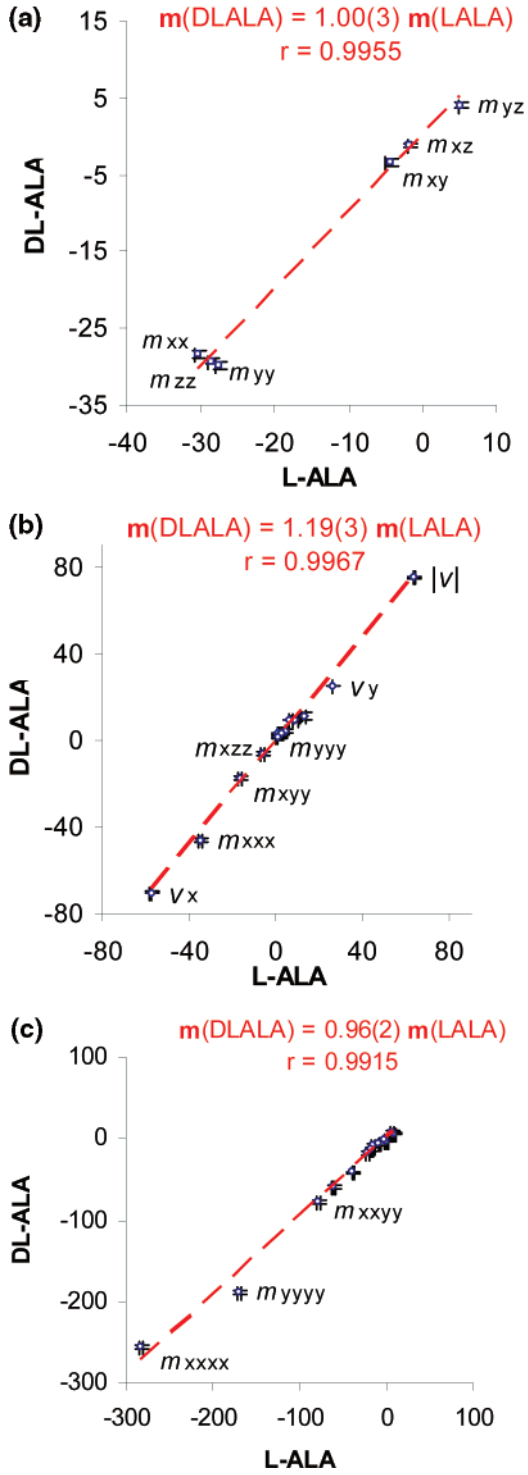

Figure 8. Linear correlation between experimental QTAIM values of the components of the in-crystal (a) second moment (in debye Å), (b) third moment (in debye Å^2), and (c) fourth moment (in debye Å^3) of LALA and DLALA. The s.u.'s are reported as vertical/horizontal bars. Where possible the labels for the individual components are indicated.

determined as a function of their separation; $E_{def-def}$ is the MM electrostatic component arising from the deformation terms of the molecular charge distribution; $E_{pro-def}$ is defined as the interaction of the spherical charge distribution of one molecule with the deformation charge density of the second. The $E_{def-def}$ part has been evaluated via the atom-centered multipole expansion up to the hexadecapole−hexadecapole term in the Cartesian tensor formulation. To check the performance of this approach, the highly accurate EP/MM method,[68] which explicitly

TABLE 6: Electrostatic Contribution (E_{es}, kJ mol^{-1}) to the Total Interaction Energies for the Three Hydrogen-Bonded Molecular Pairs of LALA and DLALA as Evaluated with Different Methods

pair[a]	crystal	d_{CM} (Å)[b]	exp1[c]	exp2[d]	MCG-BLYP[e]
A	LALA	5.7939	−135(9)	−141	−124
	DLALA	5.8388	−153(20)	−171	−121
B	LALA	4.1542	−155(8)	−171	−142
	DLALA	4.9912	−5(9)	−34	−49
C	LALA	5.1395	−23(4)	−29	−31
	DLALA	5.1399	−15(5)	−28	−32

[a] Symmetry operations relating the second molecule of a pair to the parent one (at *x*, *y*, *z*) are defined in Table 2. [b] Distance between centers of mass of the molecules in a pair. [c] Obtained from the experimental $\rho(\mathbf{r})$ through eq 4 as implemented in PAMoC (see text). The s.u. of the $E_{def-def}$ term are in parentheses. [d] Obtained from the experimental $\rho(\mathbf{r})$ adopting the EP/MM method as implemented in PAMoC (see text). [e] Obtained from MCG-BLYP calculations on the isolated dimers (program ADF, basis set TZP).

eliminates the approximations of the non-overlapping charge density inherent in the Buckingham expression, has also been used as implemented in the code PAMoC,[69] and the corresponding results are listed in the fifth column of Table 6. Furthermore, the theoretical electrostatic interaction energies obtained with the program ADF[34,35] on the isolated dimers at the crystal geometries are reported in the last column.

The following features can be noted: (1) Both the experimental estimates of the electrostatic energy describe pair A as slightly more stable in DLALA than in LALA, at variance with the theoretical result on the isolated dimer. As pair A extends along the *c* axis, i.e., along the direction of the head-to-tail packing of the molecular dipole moments, this finding is to be ascribed to the larger polarization of the charge distribution of DLALA in this direction with respect to LALA (already discussed in terms of the electric moments), which makes the charge-dipole contribution in the $E_{def-def}$ term of DLALA more attractive by 28 kJ mol^{-1} than in LALA. The feature is not reflected by the ab initio results on the isolated pair, because in the latter the crystal effects are not included. (2) All three approaches agree in describing pair B as largely more attractive in LALA than in DLALA. This is clearly the consequence of the different relative orientation of the molecules in the pair, with the antiparallel alignment in LALA strongly favored by electrostatics with respect to the parallel alignment in DLALA. In the latter, the $E_{def-def}$ term is repulsive by about 21 kJ mol^{-1}, to be compared with the strongly attractive value of −124 kJ mol^{-1} of LALA. Hence, the slightly negative value of E_{es} in DLALA is uniquely due to the attractive contribution of the promolecule energy, which is roughly constant in LALA and DLALA. (3) The additional C2−H4···O1 hydrogen bond in pair B of LALA accounts for −40 kJ mol^{-1} in the electrostatic term of the interaction energy, whereas the same interaction in DLALA is attractive by −12 kJ mol^{-1}. (4) The electrostatic repulsion between adjacent charges of the same sign in pair B of DLALA moves away the molecules involved so that the distance between their centers of mass is by 0.84 Å larger than in LALA. (5) As pair B is homochiral in LALA and heterochiral in DLALA, the difference in the corresponding values of E_{es} (in the range 135−150 kJ mol^{-1}, depending on the method used) measures the different electrostatic stability of the two aggregates in the crystal state. (6) The electrostatic interaction energies of pair C are consistently found as very similar between LALA and DLALA, reflecting in both cases the less favorable arrangement of the molecules involved and the minor strength of the formed H bond with respect to pair A. (7) As a whole, the agreement between the experimental estimates of E_{es} obtained through the new Spackman model and those from the EP/MM method can be considered more than satisfactory, although not rigorously quantitative.

TABLE 7: Lattice Energies (kJ mol^{-1}) for LALA and DLALA Crystals as Evaluated with Different Methods

crystal	exp[a]	P-B3LYP[b]
LALA	−277	−216
DLALA	−274	−215

[a] Obtained from the experimental sublimation enthalpy of LALA through eq 6. [b] Obtained with CRYSTAL03 through eq 1. Values have been corrected for BSSE.

3.8. Lattice Energies and Their Relation to Thermodynamic Properties. Lattice energies of LALA and DLALA have been obtained from their periodic ab initio electron densities through P-B3LYP calculations and compared with experimental sublimation enthalpies. It is well known that when the geometries of the molecules in the crystal and in the gas phase are identical, the lattice energy of molecular crystals is related to the sublimation enthalpy, ΔH_{sub}, as in eq 5[44]

$$E_{latt} = -\Delta H_{sub}(T) - 2RT \tag{5}$$

However, if these geometries are different, molecular deformation energy has to be considered as well. This is indeed the case for amino acids and peptides, which crystallize as zwitterions, stabilized by electrostatic, polarization, and H-bonding intermolecular interactions, and change to neutral form in the gas phase (upon sublimation), through intramolecular proton transfer. The energy required for this process is known as the relaxation energy, E_{rel}, and is obtained as the difference between the ab initio molecular energy of the gas (neutral form) and the crystal (zwitterionic form). It must be accounted for, and the eq 5 is changed into eq 6

$$E_{latt} = -\Delta H_{sub}(T) - 2RT + E_{rel} \tag{6}$$

Our estimates for E_{rel} of LALA and DLALA, obtained through DFT optimizations (MG-B3LYP/DZP) starting from the X-ray geometries and ending at the same conformer, provide values of −137 and −134 kJ mol^{-1} for LALA and DLALA, respectively, in good agreement with previously reported results.[44] Experimental sublimation enthalpies are available from the literature only for LALA: the value reported is obtained from the temperature dependence of vapor pressure and amounts to ΔH_{sub} (414 K) = (132.8 ± 1) kJ mol^{-1}.[70] As previously done by other authors,[71] we assume the experimental value for LALA to provide a reasonable basis for comparison also for DLALA, relying on the fact that the difference between sublimation enthalpies of racemates and enantiomorphs is generally small.[7,8,11] By insertion of this value in eq 6 we obtain for LALA and DLALA values of the calorimetric lattice energies equal to −277 and −274 kJ mol^{-1}, respectively. They are compared in Table 7 with our theoretical P-B3LYP estimates obtained with the code CRYSTAL03 (see section 2.2). It can be seen that: (1) P-B3LYP results underestimate by about 21% the calorimetric data. This is in line with what is found by other authors[46b,71] on some organic molecular crystals and confirms that DFT calculations do not properly include dispersion energies.[72] (2) Irrespective of the miscalculated values, the theoretical estimates predict crystals of LALA and DLALA as equally thermodynamically favored, further supporting what is anticipated by means of

thermochemical measurements on some racemic and chiral crystals.[8,11,71]

To overcome the inadequacy of the theoretical calculations, attempts to obtain reasonable estimates of the lattice energies have been recently based on the experimental charge densities (which intrinsically include correlation effects such as dispersion), by a method[73] often referred to as experimental charge density approach (ECDA) to intermolecular interactions.[13b,21,54,71,74] However, while the electrostatic contribution to the total interaction energies can be rigorously treated (see the preceding section) within this approach, the other terms in the force field, i.e., the dispersion and the exchange−repulsion terms, are estimated through various atom−atom potential functions, whose choice is to some extent arbitrary and parameter-dependent. For both LALA and DLALA, we have obtained values of the lattice energies that change by up to 80%, depending on the selected atom−atom potential. Therefore, it appears that these force field terms are currently not appropriate to derive reliable estimates of the lattice energies and have to be improved, as recently suggested.[67] Some attempts in this direction, using suitable scaling to the proper energetic terms in the Morokuma−Ziegler decomposition scheme,[75,76] are currently in progress in our laboratory.[77] All this suggested to confine our investigation of the X-ray-derived lattice energies for LALA and DLALA to the electrostatic contributions only. We have found E_{es} values of −315 and −99 kJ mol^{-1} through the EP/MM method applied to LALA and DLALA, respectively, which point to a marked electrostatic dissimilarity between the two crystals. However, an additional crucial point has to be considered in the case of DLALA, because of its polar space group $Pna2_1$, with molecular dipoles parallel-aligned along the *c* axis. A supplementary term for the Coulombic energy, as derived by an integration over a uniform distribution of dipolar unit cells, must be evaluated.[65,78] Our estimate of this additional term for DLALA is as large as −170 kJ mol^{-1}, which, added to the quantity obtained through the EP/MM method, makes the electrostatic lattice energy of DLALA attractive by −269 kJ mol^{-1}. These results show that, notwithstanding the equal thermodynamic stability of LALA and DLALA indicated by the P-B3LYP values of E_{latt}, the two crystal forms are significantly different from an electrostatic point of view, and the diverse orientation of the dipole vectors in the unit cells makes the crystals of LALA more electrostatically stable by 46 kJ mol^{-1} than the crystals of DLALA. Li and co-workers,[4,9] who studied the relationship between physical properties of chiral and racemic drugs, observed that a larger electrostatic stability corresponds to a higher melting point. In our case, this relationship cannot be inferred, since the melting points of LALA and DLALA, as for most amino acids, are not well defined, due to decomposition at high temperature.

4. Conclusions

We have shown that the investigation of the charge density distributions of an enantiomer and its corresponding racemic compound offers a unique opportunity to characterize the interactions of the same molecule in different crystalline environments and to explore the extent of the $\rho(\mathbf{r})$ transferability. In this study, the accurate, low-temperature $\rho(\mathbf{r})$ distributions of zwitterionic LALA and DLALA have been compared and relevant parameters to distinguish between the two crystal forms have been obtained, bringing out differences and similarities in terms of (i) geometric descriptors, (ii) topological indexes, (iii) molecular $\Phi(\mathbf{r})$ distributions, (iv) atomic volumes and charges, (v) molecular electric moments, and (vi) electrostatic interaction energies.

In particular, we have found that:

(1) The molecular conformation of the alanine molecule is slightly but significantly altered by the different intermolecular environment in crystals of LALA and DLALA, while the hydrogen-bonding motifs in the two crystals are almost identical on both geometrical and topological grounds.

(2) Local topological indexes of both covalent bonds and intermolecular H bonds spread over a narrow range and are therefore generally transferable between LALA and DLALA.

(3) The electrostatic consequences of the different packing in LALA and DLALA are revealed by the comparison of the molecular $\Phi(\mathbf{r})$ distributions. In particular, differences in the molecular surface shapes and in the position of the maxima of $\Phi(\mathbf{r})$ are evidenced, suggesting that the likely direction of approach of nucleophilic reactants are diverse for the two crystal structures.

(4) In-crystal QTAIM group charges are transferable between LALA and DLALA, while corresponding group volumes are not (not strictly).

(5) Molecular first and third moments indicate that for the zwitterionic alanine molecule the molecular charge distribution in DLALA is more polarized in the *c* direction by about 10%. The components of the tensors are not strictly transferable. Conversely, second and fourth moments are unaltered, suggesting a marked similarity of these properties in the two crystals.

(6) Significant differences arise from the packing of the dipole vectors in the two crystals, which are aligned in an *antiparallel* fashion in LALA, to be compared with a *parallel* alignment in DLALA, due to its space group $Pna2_1$. As a consequence, the electrostatic energy is significantly more attractive in LALA than in DLALA.

(7) Homochiral (LL) intermolecular interactions between alanine molecules are found to be more electrostatically stable by 135−150 kJ mol^{-1} than heterochiral (DL) interactions.

(8) In the evaluation of the Coulombic energy for the polar DLALA crystal, the term arising from the nonzero dipole moment of the unit cell amounts to more than 60% of the total electrostatic lattice energy.

(9) Theoretical P-B3LYP estimates of the crystal lattice energies predict LALA and DLALA as equally thermodynamically favored, even if the comparison with the experimental sublimation enthalpies has shown that a better account of the correlation effects is needed.

(10) To obtain reliable estimates of the experimental lattice energies through the ECDA to intermolecular interactions, some improvement in the description of the dispersion and the exchange−repulsion terms is required.

To the best of our knowledge, this is the first paper in which the experimental $\rho(\mathbf{r})$ of related chiral compounds are compared, providing an ideal test of the transferability of electron densities and derived parameters.

Supporting Information Available: A complete description of the DLALA data treatment, together with full lists of experimental bond distances, bond angles, and torsion angles of LALA and DLALA at 23 and 19 K, respectively. Full lists of the theoretical optimized coordinates. Full list of the experimental topological indicators at the bcps of all the covalent bonds. Tables of the individual QTAIM atomic volumes and charges. Tables of the experimental QTAIM molecular second, third, and fourth moments. Contour maps of the residual electron densities in the plane of the COO^- moieties. This information is available free of charge via the Internet at http:// pubs.acs.org.

References and Notes

(1) Dunitz, J. D. *Pure Appl. Chem.* **1991**, *63*, 177−185.

(2) (a) Bernstein, J. *Polymorphism in Molecular Crystals*; Oxford University press: Oxford, 2002. (b) Bernstein, J.; Davey, R. J.; Henck, J.-O. *Angew. Chem., Int. Ed.* **1999**, *38*, 3440−3461.

(3) For the proper definition of the terms "homochiral" and "heterochiral" see: Thomson, W. *Baltimore Lectures on Molecular Dynamics and Wave Theory of Light*; C. J. Clay & Sons: London, 1904; p 619.

(4) Li, Z. J.; Grant, D. J. W. *J. Pharm. Sci.* **1997**, *86*, 1073−1078.

(5) (a) Sen, S.; Yu, P.; Risbud, S. H.; Dick, R.; Deamer, D. *J. Phys. Chem. B* **2006**, *110*, 18058−18063. (b) Kitchin, S. J.; Tutoveanu, G.; Steele, M. R.; Porter, E. L.; Harris, K. D. M. *J. Phys. Chem. B* **2005**, *109*, 22808−22813.

(6) Larsen, S.; Marthi, K. *Acta Crystallogr.* **1997**, *B53*, 280−292.

(7) (a) Sørensen, H. O.; Larsen, S. *Acta Crystallogr.* **2003**, *B59*, 132−140. (b) Larsen, S.; Marthi, K. *Acta Crystallogr.* **1997**, *B53*, 803−811.

(8) Perlovich, G. L.; Kurkov, S. V.; Hansen, L. Kr.; Bauer-Brandl, A. *J. Pharm. Sci.* **2004**, *93*, 654−666.

(9) Li, Z. J.; Ojala, W. H.; Grant, D. J. W. *J. Pharm. Sci.* **2001**, *90*, 1523−1539.

(10) Wallach, O. *Liebigs Ann. Chem.* **1895**, *286*, 90−143.

(11) Brock, C. P.; Schweizer, W. B.; Dunitz, J. D. *J. Am. Chem. Soc.* **1991**, *113*, 9811−9820.

(12) Huang, J.; Yu, L. *J. Am. Chem. Soc.* **2006**, *128*, 1873−1878.

(13) (a) Overgaard, J.; Waller, M. P.; Piltz, R.; Platts, J. A.; Emseis, P.; Leverett, P.; Williams, P. A.; Hibbs, D. E. *J. Phys. Chem. A* **2007**, 111, 10123−10133. (b) Munshi, P.; Guru Row, T. N. *Cryst. Growth Des.* **2006**, *6*, 708−718. (c) Hibbs, D. E.; Overgaard, J.; Platts, J. A.; Walker, M. P.; Hursthouse, M. B. *J. Phys. Chem. B* **2004**, *108*, 3663−3672. (d) Whitten, A. E.; Dittrich, B.; Spackman, M. A.; Turner, P.; Brown, T. C. *Dalton Trans.* **2004**, 23−29. (e) Gopalan, R. S.; Kulkarni, G. U.; Rao, C. N. R. *Chem. Phys. Chem.* **2000**, *1*, 127−135.

(14) Pichon-Pesme, V.; Lecomte, C.; Lachekar, H. *J. Phys. Chem.* **1995**, *99*, 6242−6250.

(15) Jelsch, C.; Teeter, M. M.; Lamzin, V.; Pichon-Pesme, V.; Blessing, R. H.; Lecomte, C. *Proc. Natl. Acad. Sci. U.S.A.* **2000**, *97*, 3171− 3176.

(16) Lecomte, C.; Guillot, B.; Jelsch, C.; Podjarny, A. *Int. J. Quantum Chem.* **2005**, *101*, 624−634.

(17) O'Brien, S. E.; Popelier, P. L. A. *Can. J. Chem.* **1999**, *77*, 28−36.

(18) Matta, C. F.; Bader, R. F. W. *Proteins Struct. Funct. Genet.* **2003**, *52*, 360−399.

(19) Dittrich, B.; Scheins, S.; Paulmann, C.; Luger, P. *J. Phys. Chem. A* **2003**, *107*, 7471−7474.

(20) Bader, R. F. W. *Atoms in molecules: a quantum theory*; Oxford University Press: Oxford, 1990.

(21) Overgaard, J.; Hibbs, D. E. *Acta Crystallogr.* **2004**, *A60*, 480−487.

(22) Walker, P.; Arteca, G.; Mezey, P. *J. Comput. Chem.* **1991**, *12*, 220−230.

(23) Bohorquez, H. J.; Obregón, M.; Cárdenas, C.; Llanos, E.; Suárez, C.; Villaveces, J. L.; Patarroyo, M. E. *J. Phys. Chem. A* **2003**, *107*, 10090−10097.

(24) Parkin, A.; Barr, G.; Dong, W.; Gilmore, C. J.; Jayatilaka, D.; McKinnon, J. J.; Spackman, M. A.; Wilson, C. C. *Cryst. Eng. Commun.* **2007**, *9*, 648−652.

(25) (a) Nandhini, M. S.; Krishnakumar, R. V.; Natarajan, S. *Acta Crystallogr.* **2001**, *C57*, 614−615. (b) Donohue, J. *J. Am. Chem. Soc.* **1950**, *72*, 949−953. (c) Levy, H. A.; Corey, R. B. *J. Am. Chem. Soc.* **1941**, *63*, 2095−2108.

(26) Simpson, H. J., Jr.; Marsh, R. E. *Acta Crystallogr.* **1966**, *20*, 550−555.

(27) (a) Gatti, C.; Bianchi, R.; Destro, R.; Merati, F. *THEOCHEM* **1992**, *255*, 409−433. (b) Destro, R.; Bianchi, R.; Gatti, C.; Merati, F. *Chem. Phys. Lett.* **1991**, *186*, 47−52. (c) Destro, R.; Bianchi, R.; Morosi, G. *J. Phys. Chem.* **1989**, *93*, 4447−4457. (d) Destro, R.; Marsh, R. E., Bianchi, R. *J. Phys. Chem.* **1988**, *92*, 966−973.

(28) Roversi, P.; Destro, R. *Chem. Phys. Lett.* **2004**, *386*, 472−478.

(29) (a) Stewart, R. F. *J. Chem. Phys.* **1969**, *51*, 4569−4577. (b) Stewart, R. F. *Acta Crystallogr.* **1976**, *A32*, 565−574. (c) Stewart, R. F. In *The Applications of Charge Density Research to Chemistry and Drug Design*; Jeffrey, G. A., Piniella, J. F., Eds.; Plenum Press: New York, 1991; pp 63−101.

(30) Destro, R. *Aust. J. Phys.* **1988**, *41*, 503−510.

(31) Samson, S.; Goldish, E.; Dick, C. J. *J. Appl. Crystallogr.* **1980**, *13*, 425−432.

(32) Stewart, R. F.; Spackman, M. A.; Flensburg, C. *VALRAY User's Manual*, version 2.1; Carnegie Mellon University and University of Copenhagen, 2000.

(33) (a) Whitten, A. E.; Turner, P.; Klooster, W. T.; Piltz, R. O.; Spackman, M. A. *J. Phys. Chem. A* **2006**, *110*, 8763−8776. (b) Madsen, A. Ø.; Sørensen, H. O.; Flensburg, C.; Stewart, R. F.; Larsen, S. *Acta Crystallogr.* **2004**, *A60*, 550−561.

(34) Te Velde, G.; Bickelhaupt, F. M.; Baerends, E. J.; Fonseca Guerra, C.; Van Gisbergen, S. J. A.; Snijders, J. G.; Ziegler, T. *J. Comput. Chem.* **2001**, *22*, 931−967.

(35) *ADF2004.01*, SCM; Vrije Universiteit: Amsterdam, The Netherlands (http://www.scm.com).

(36) Becke, A. D. *Phys. Rev. A* **1988**, *38*, 3098−3100.

(37) Lee, C.; Yang, W.; Parr, R. G. *Phys. Rev. B* **1988**, *37*, 785−789.

(38) Boys, S. F.; Bernardi, F. *Mol. Phys.* **1970**, *19*, 553−566.

(39) Frisch, M. J.; Trucks, G. W.; Schlegel, H. B.; Scuseria, G. E.; Robb, M. A.; Cheeseman, J. R.; Zakrzewski, V. G.; Montgomery J. A., Jr.; Stratmann, R. E.; Burant, J. C.; Dapprich, S.; Millam, J. M.; Daniels, A. D.; Kudin, K. N.; Strain, M. C.; Farkas, O.; Tomasi, J.; Barone, V.; Cossi, M.; Cammi, R.; Mennucci, B.; Pomelli, C.; Adamo, C.; Clifford, S.; Ochterski, J.; Petersson, G. A.; Ayala, P. Y.; Cui, Q.; Morokuma, K.; Rega, N.; Salvador, P.; Dannenberg, J. J.; Malick, D. K.; Rabuck, A. D.; Raghavachari, K.; Foresman, J. B.; Cioslowski, J.; Ortiz, J. V.; Baboul, A. G.; Stefanov, B. B.; Liu, G.; Liashenko, A.; Piskorz, P.; Komaromi, I.; Gomperts, R.; Martin, R. L.; Fox, D. J.; Keith, T.; Al-Laham, M. A.; Peng, C. Y.; Nanayakkara, A.; Challacombe, M.; Gill, P. M. W.; Johnson, B.; Chen, W.; Wong, M. W.; Andres, J. L.; Gonzalez, C.; Head-Gordon, M.; Replogle, E. S.; Pople, J. A. *Gaussian 98*, revision A.11.3; Gaussian, Inc., Pittsburgh, PA, 2002.

(40) Becke, A. D. *J. Chem. Phys.* **1993**, *98*, 5648−5652.

(41) Thakkar, A. J.; Koga, T.; Saito, M.; Hoffmeyer, R. E. *Int. J. Quantum Chem., Quantum Chem. Symp.* **1993**, *27*, 343−354.

(42) Koga, T.; Thakkar, A. J. *Theor. Chim. Acta* **1993**, *85*, 391−394.

(43) Voogd, J.; Derissen, J. L.; Duijneveldt, F. B. *J. Am. Chem. Soc.* **1981**, *103*, 7701−7706.

(44) Bisker-Leib, V.; Doherty, M. F. *Cryst. Growth Des.* **2003**, *3*, 221−237.

(45) Saunders, V. R.; Dovesi, R.; Roetti, C.; Orlando, R.; Zicovich-Wilson, C. M.; Harrison, N. M.; Doll, K.; Civalleri, B.; Bush, I. J.; D'Arco, Ph.; Llunell, M. *CRYSTAL2003 User's Manual*; University of Torino: Torino, 2003.

(46) (a) Spackman, M. A.; Mitchell, A. S. *Phys. Chem. Chem. Phys.* **2001**, *3*, 1518−1523. (b) Perger, W. F.; Pandey, R.; Blanco, M. A.; Zhao, J. *Chem. Phys. Lett.* **2004**, *388*, 175−180.

(47) Barzaghi, M. *PAMoC (Version 2002.0), Online User's Manual*; CNR-ISTM, Institute of Molecular Science and Technologies: Milano, Italy 2002; http://www.istm.cnr.it/pamoc/.

(48) (a) Biegler-König, F. W.; Bader, R. F. W.; Tang, T.-H. *J. Comput. Chem.* **1982**, *3*, 317−328. (b) AIMPAC download page: http://www.chemistry.mcmaster.ca/aimpac/imagemap/imagemap.htm.

(49) Obtained with the following software: Brandenburg, K.; Putz, H. *Diamond - Crystal and Molecular Structure Visualization 3.1d*; Crystal Impact GbR: Bonn, 2006; http://www.crystalimpact.com/diamond.

(50) Gatti, C. *Z. Kristallogr.* **2005**, *220*, 399−457.

(51) Koritsanszky, T. S.; Coppens, P. *Chem. Rev.* **2001**, *101*, 1583−1627.

(52) Kirzhnits, D. A. *Sov. Phys. JETP* **1957**, *5*, 64−71.

(53) Abramov, Y. A. *Acta Crystallogr.* **1997**, *A53*, 264−272.

(54) Soave, R.; Barzaghi, M.; Destro, R. *Chem.−Eur. J.* **2007**, *13*, 6942−6956.

(55) Politzer, P.; Murray, J. S.; Peralta-Inga, Z. *Int. J. Quantum Chem.* **2001**, *85*, 676−684.

(56) Hübschle, C. B.; Luger, P. *J. Appl. Cryst.* **2006**, *39*, 901−904.

(57) Bader, R. F. W.; Caroll, M. T.; Cheeseman, J. R.; Chang, C. *J. Am. Chem. Soc.* **1987**, *109*, 7968−7979.

(58) Li, X.; Wu, G.; Abramov, Y. A.; Volkov, A. V.; Coppens, P. *PNAS* **2002**, *99*, 12132−12137.

(59) Rödel, E.; Messerschmidt, M.; Dittrich, B.; Luger, P. *Org. Biomol. Chem.* **2006**, *4*, 475−481.

(60) Lorenzo, L.; González Moa, M. J.; Mandado, M.; Mosquera, R. A. *J. Chem. Inf. Model.* **2006**, *46*, 2056−2065.

(61) QTAIM performs a topological analysis of $\rho(\mathbf{r})$ and divides all space into nonoverlapping regions separated by surfaces on which $\nabla\rho(\mathbf{r})\cdot\mathbf{n}$ is zero, where $\mathbf{n}$ is a vector normal to the surfaces.

(62) Spackman, M. A. *Chem. Rev.* **1992**, *92*, 1769−1797.

(63) McLean, A. D.; Yoshimine, M. *J. Chem. Phys.* **1967**, *47*, 1927−1935.

(64) Destro, R.; Roversi, P.; Barzaghi, M.; Marsh, R. E. *J. Phys. Chem. A* **2000**, *104*, 1047−1054.

(65) Gavezzotti, A. *Molecular Aggregation*; Oxford University Press: New York, 2007.

(66) (a) Buckingham, A. D. In *Physical Chemistry. An Advanced Treatise*; Henderson, D., Ed.; Academic Press, New York, 1970; pp 349−386. (b) Buckingham, A. D. In *Intermolecular Interactions: From Diatomics to Biopolymers*; Pullmann, B., Ed.; Wiley and Sons: Chichester, New York, 1978; pp 1−67.

(67) Spackman, M. A. *Chem. Phys. Lett.* **2006**, *418*, 158−162.

(68) (a) Volkov, A.; Coppens, P. *J. Comp. Chem*. **2004**, *25*, 921−934. (b) Volkov, A.; Koritsanszky, T.; Coppens, P. *Chem. Phys. Lett*. **2004**, *391*, 170−175.

(69) PAMoC, as a default, evaluates the electrostatic contribution to the intermolecular interaction energies as the sum of the Buckingham MM term and the $E_{pro-pro}$ term, following ref 67. On the other hand, when the EP/MM option is set, PAMoC switches to the exact EP method whenever the interatomic distance is lower than the sum of van der Waals radii or the $E_{pro-pro}$ value is lower than −0.5 kJ/mol. By these criteria, the agreement between the EP/MM and EP results is almost quantitative.

(70) De Kruif, C. G.; Voogd, J.; Offringa, J. C. A. *J. Chem. Thermodyn*. **1979**, *11*, 651−656.

(71) Abramov, Y. A.; Volkov, A.; Wu, G.; Coppens, P. *J. Phys. Chem. B* **2000**, *104*, 2183−2188.

(72) Van Mourik, T.; Gdanitz, R. J. *J. Chem. Phys*. **2002**, *116*, 9620−9623.

(73) (a) Spackman, M. A.; Weber, H. P.; Craven, B. M. *J. Am. Chem. Soc*. **1988**, *110*, 775−782. (b) Spackman, M. A. *J. Chem. Phys*. **1986**, *85*, 6579−6586. (c) Spackman, M. A. *J. Chem. Phys*. **1986**, *85*, 6587−6601. (d) Spackman, M. A. *J. Phys. Chem.* **1987**, *91*, 3179−3186.

(74) Abramov, Y. A.; Volkov, A.; Wu, G.; Coppens, P. *Acta Crystallogr*. **2000**, *A56*, 585−591.

(75) Ziegler, T.; Rauk, A. *Theor. Chim. Acta* **1977**, *46*, 1−10.

(76) Morokuma, K. *J. Chem. Phys*. **1971**, *55*, 1236−1244.

(77) Barzaghi, M.; Soave, R.; Destro, R. In preparation.

(78) Van Eijck, B. P.; Kroon, J. *J. Phys. Chem. B* **1997**, *101*, 1096−1100.